

<Supporting Information>

A stable Cd-MOF as a dual-responsive luminescent biosensor for determination of urinary diphenyl phosphate and hippuric acid as biomarkers for human triphenyl phosphate and toluene poisoning

Mingyuan Lei,^a Fayuan Ge,^a Tingting Wu,^a Xinde Duan,^a Zhiqiang Shi^b and Hegen

Zheng*^a

^aState Key Laboratory of Coordination Chemistry, School of Chemistry and Chemical Engineering, Collaborative Innovation Center of Advanced Microstructures, Nanjing University, Nanjing 210023, P. R. China

^bSchool of Chemistry and Chemical Engineering, Suzhou University, Suzhou 234000, PR China

Email: zhenghg@nju.edu.cn

Section S1. Materials and Measurements

All chemicals were of analytical grade and used without further purification. Bibpdx ligand was synthesized in accordance with the literature procedure.^{S1} Infrared spectra were recorded on a Bruker Tensor 27 spectrometer in the 4000-400 cm^{-1} region. Thermogravimetric analyses (TGA) was performed under nitrogen atmosphere with a heating rate of 10 $^{\circ}\text{C min}^{-1}$ using a Netzsch STA 449 F3 thermal analyzer. The powder X-ray diffraction (PXRD) patterns were recorded on a Bruker D8 Advance diffractometer with Cu $K\alpha$ radiation ($\lambda = 1.5418 \text{ \AA}$) at room temperature. The photoluminescence spectra were obtained by Hitachi F-4600 fluorescence spectrophotometer. Bright-field optical images and fluorescence microscopy images were taken from a Leica DMI8 inverted fluorescence microscope. The lifetime measurements were measured on a Horiba Jobin Yvon Fluorolog-3 spectrofluorometer. The UV-vis absorption spectra were recorded by using a Shimadzu UV-3600 double monochromator spectrophotometer.

Section S2. X-ray Crystallography

Single-crystal X-ray diffraction data were collected on a Bruker Apex Smart CCD diffractometer with graphite-monochromated Mo $K\alpha$ ($\lambda = 0.71073 \text{ \AA}$) radiation at room temperature. The structures were solved by direct methods and refined with full-matrix least-squares on F^2 using the SHELX-2018/3 program package.^{S2} All non-hydrogen atoms were refined with anisotropic displacement parameters, while the hydrogen atoms on ligands were placed in idealized positions with isotropic thermal parameters. The hydrogen atoms on urea groups and water molecules were found from the different Fourier maps, while the hydrogen atoms attached to carbon atoms were generated geometrically and refined by using a riding mode. There are large solvent accessible pore volumes in the structure of comolex **1**, which are occupied by highly disordered solvent molecules. No satisfactory disorder model for these solvent molecules could be achieved, and therefore the SQUEEZE program implemented in PLATON was used to remove these electron densities of these disordered species.^{S3} Thus, all of electron densities from free solvent molecules have been “squeezed” out. The electron count within the solvent accessible void (calculated using the SQUEEZE

algorithm within PLATON) measured 119 electrons per unit cell, corresponding to two DMF molecule and four H₂O molecules per unit cell, confirmed by TG analysis. Crystal and refinement data are summarized in Table S1, the selected bond lengths and bond angles are listed in Tables S2. CCDC 2169017 contains the supplementary crystallographic data for this paper.

Table S1. Crystal data and structure refinement parameters for **1**.

	1
Empirical formula	C ₃₄ H ₂₆ N ₆ O ₅ Cd
Formula weight	711.01
Crystal system	Triclinic
Space group	<i>P</i> $\bar{1}$
<i>a</i> (Å)	10.3016(4)
<i>b</i> (Å)	11.3105(4)
<i>c</i> (Å)	18.0656(6)
<i>V</i> (Å ³)	1887.33(12)
<i>α</i> (°)	72.101(2)
<i>β</i> (°)	89.930(2)
<i>γ</i> (°)	71.389(2)
<i>Z</i>	2
ρ_{calcd} (g·cm ⁻³)	1.251
<i>F</i> (000)	720
θ range (°)	1.865 to 28.562
Index ranges	-12 ≤ <i>h</i> ≤ 12, -14 ≤ <i>k</i> ≤ 14, -21 ≤ <i>l</i> ≤ 22
Data/restraints/parameters	7684/0/415
GOF on <i>F</i> ²	0.970
<i>R</i> ₁ ^{<i>a</i>} , <i>wR</i> ₂ ^{<i>b</i>} [<i>I</i> > 2σ(<i>I</i>)]	0.0490, 0.1216
<i>R</i> ₁ ^{<i>a</i>} , <i>wR</i> ₂ ^{<i>b</i>} [all data]	0.0648, 0.1314

$$^a R_1 = \sum ||F_o| - |F_c|| / \sum |F_o|; ^b wR_2 = \{ \sum [w(F_o^2 - F_c^2)^2] / \sum [w(F_o^2)^2] \}^{1/2}.$$

Table S2. Selected bond lengths (Å) and angles (°) for **1**.

Bond lengths			
Cd1—O1	2.319(3)	Cd1—O2B	2.284(4)
Cd1—O3A	2.313(3)	Cd1—O4A	2.370(3)
Cd1—N3	2.276(4)	Cd1—N6C	2.263(4)
Bond angles			
O1—Cd1—O2B	120.33(14)	O1—Cd1—O3A	94.34(12)
O1—Cd1—O4A	148.93(13)	O1—Cd1—N3	83.76(14)
O1—Cd1—N6C	90.51(14)	O2B—Cd1—O3A	143.93(11)
O2B—Cd1—O4A	89.97(13)	O2B—Cd1—N3	83.62(15)
O2B—Cd1—N6C	101.05(15)	O3A—Cd1—O4A	54.66(10)
O3A—Cd1—N3	91.21(13)	O3A—Cd1—N6C	87.25(12)
O4A—Cd1—N3	93.82(13)	O4A—Cd1—N6C	90.07(12)
N3—Cd1—N6C	173.94(14)		

Symmetry codes: A: $-x+2, -y+1, -z+1$; B: $-x+1, -y+1, -z+1$; C: $x, y+1, z-1$.

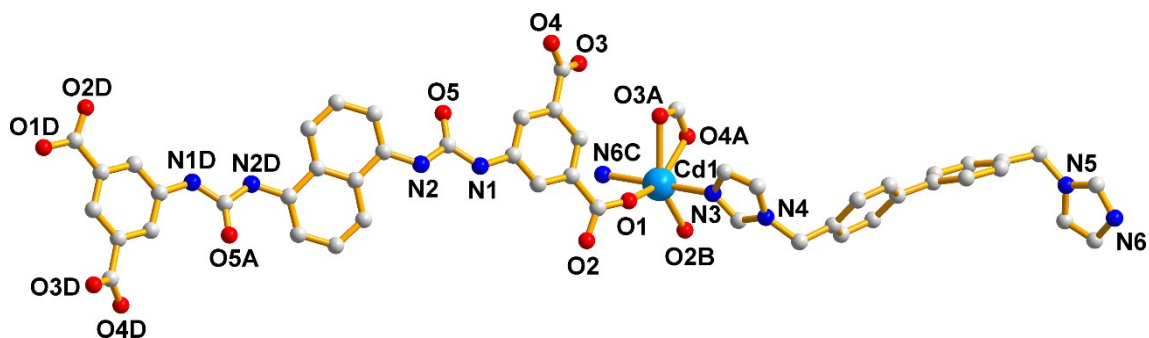
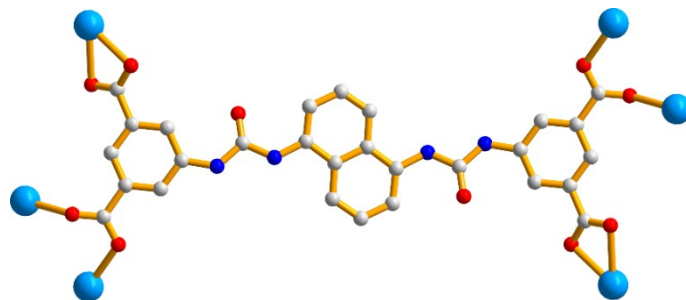
**Fig. S1** Coordination environment of Cd^{2+} in complex **1** (Symmetry codes: A: $-x+2, -y+1, -z+1$; B: $-x+1, -y+1, -z+1$; C: $x, y+1, z-1$; D: $-x+1, -y+3, -z$).

Fig. S2 Coordination mode of L^{4-} ligand in complex **1**.

Section S3. Thermal Gravimetric Analysis

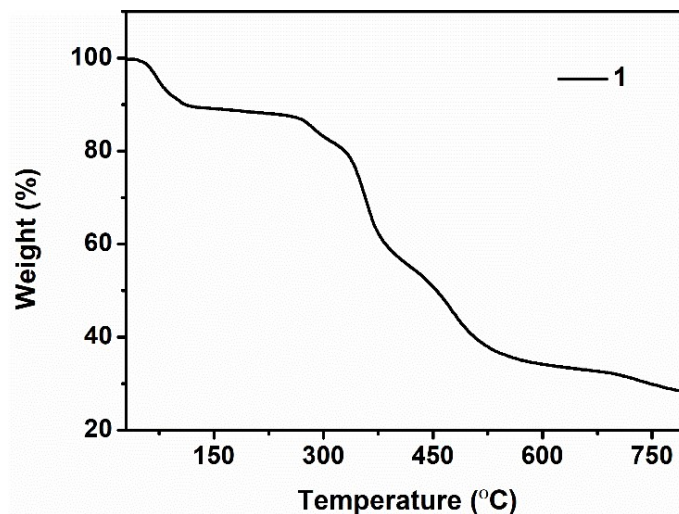


Fig. S3 The TGA curve of **1** under nitrogen atmosphere. The TGA curve of **1** shows an initial weight loss of 12.85% (calculated: 13.30%), which may be attributed to loss of one lattice DMF molecule and two water molecules. This result is also consistent with the result of the SQUEEZE analysis in PLATON.

Section S4. Luminescence Sensing

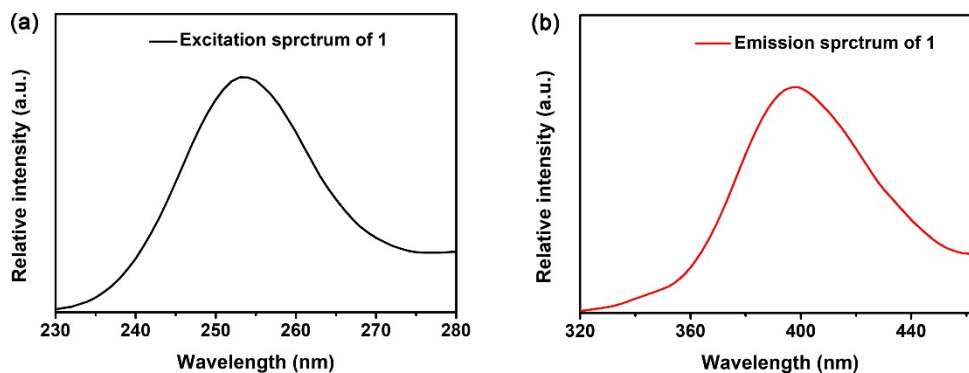


Fig. S4 The excitation and emission spectra of **1** in solid state. Complex **1** displayed the emission at 400 nm upon excitation at 250 nm.

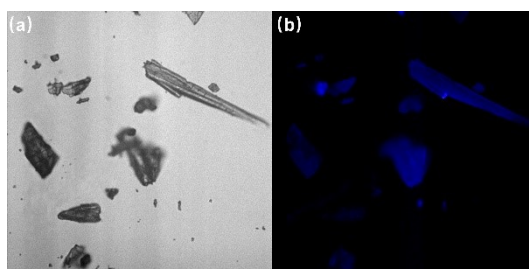


Fig. S5 Digital photographs of **1** under normal light and upon excitation.

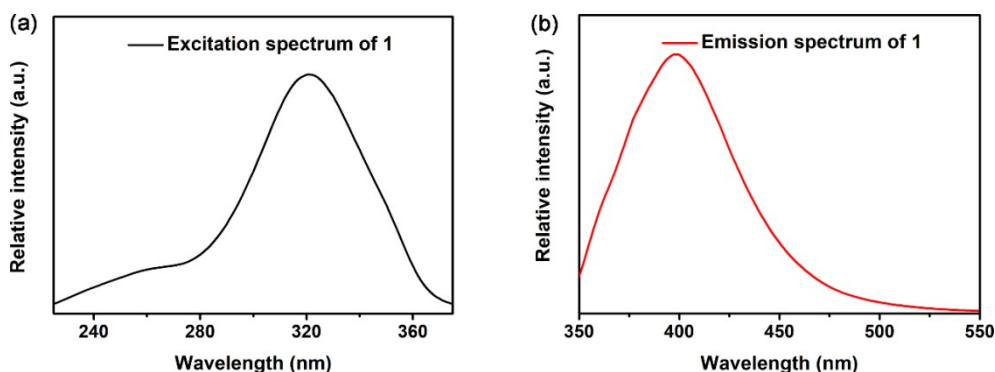


Fig. S6 The excitation and emission spectra of **1** in water.

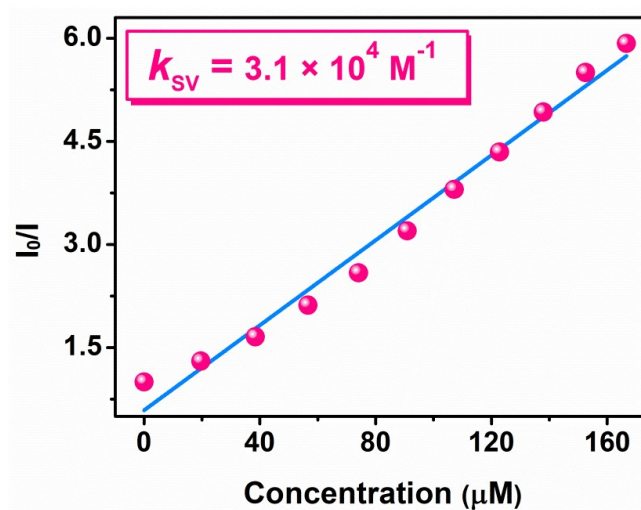


Fig. S7 S-V plot of I_0/I vs. DPP concentration in water.

Table S3. LODs and response rates for the reported materials for DPP and HA.

Materials	Analysts	LOD (μM)	Response rate	Ref.
$\{[\text{NH}_2(\text{CH}_3)_2]_2 \cdot [\text{Cd}_{3.5}(\text{bdba})(\text{Hbdba})(\text{H}_2\text{O})_{1.5}]\}_n$	DPP	87.94	1.5 min	[S4]
$[\text{Cd}(\text{L})(\text{BPDC})_{0.5}\text{H}_2\text{O}] \cdot 0.5\text{H}_2\text{O}$	HA	17.87	/	[S5]
$[\text{Zn}_2(\text{L})_2(\text{BPDC})] \cdot 2\text{H}_2\text{O}$	HA	22.59	/	[S5]
$[\text{Cd}_2(\text{L})(\text{BTC})\text{H}_2\text{O}] \cdot 3\text{H}_2\text{O}$	HA	28.15	/	[S5]
$\text{Eu}^{3+}@\text{MIL-121}$	HA	50.23	10 min	[S6]
$\text{MIL-124}@\text{Eu}^{3+}$	HA	45.21	/	[S7]
$\text{CC}[4]\text{A}@\text{MIL-53-NH}_2(\text{Al})$	HA	20.65	/	[S8]

$\{[\text{Cd}(\text{L})_{0.5}(\text{bpbix})] \cdot x(\text{solv})\}_n$	DPP	1.09	1 min	This
	HA	1.09	1 min	work

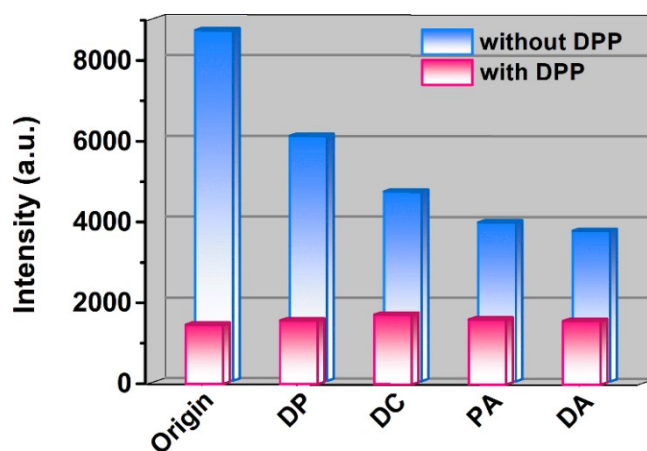


Fig. S8 The luminescence intensities of **1** after addition of DPP ($166.7 \mu\text{M}$) in the existence of other compounds ($166.7 \mu\text{M}$) with similar structure to DPP (diphenyl phosphite (DP), diphenyl chlorophosphite (DC), phenylphosphonic acid (PA), diphenylphosphinic acid (DA)).

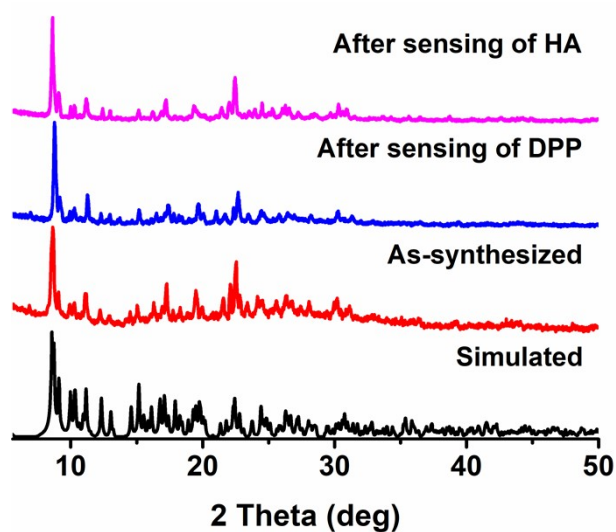


Fig. S9 PXRD of **1** and samples of **1** after the cycling sensing experiments of DPP and HA.

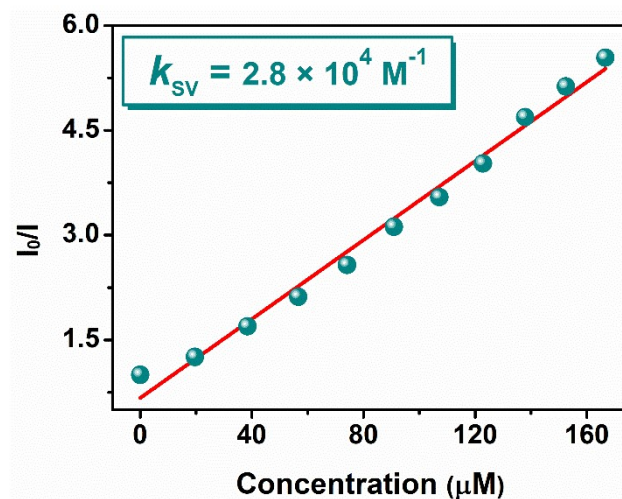


Fig. S10 S-V plot of I_0/I vs. HA concentration in water.

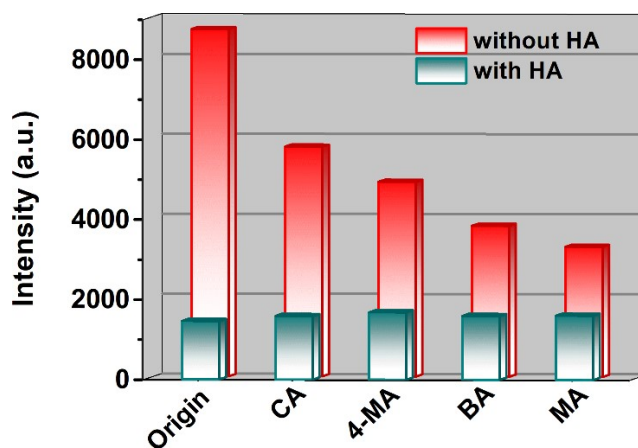


Fig. S11 The luminescence intensities of **1** after addition of HA (166.7 μM) in the existence of other compounds (166.7 μM) with similar structure to HA (2-[(4-chlorobenzoyl)amino]acetic acid (CA), 4-methylhippuric acid (4-MA), N-benzoyl-DL-alanine (BA), mandelic acid (MA)).

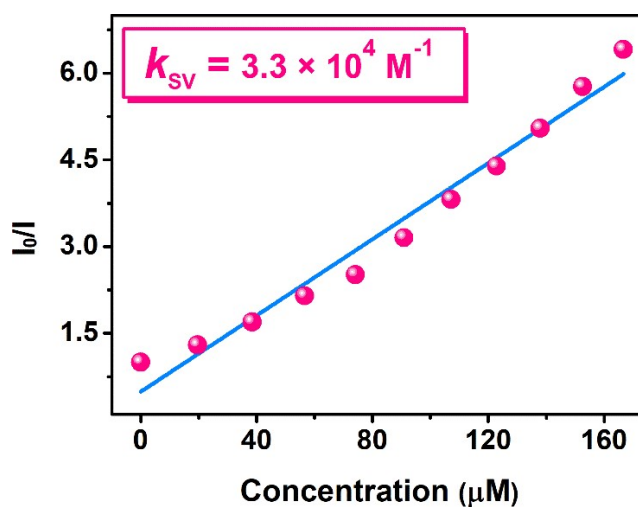


Fig. S12 S-V plot of I_0/I vs. DPP concentration in urine.

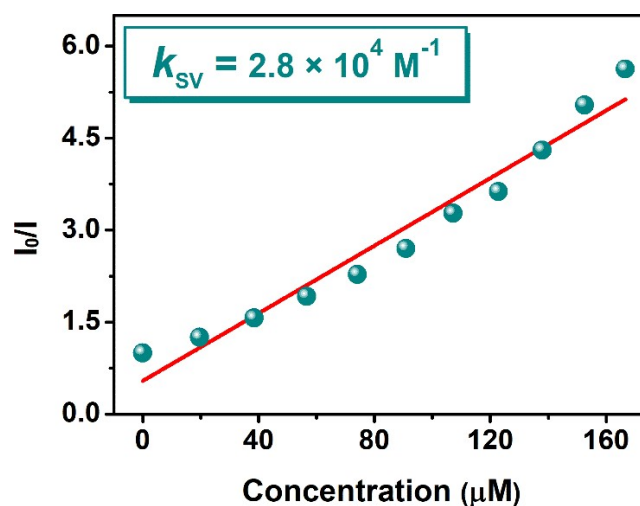


Fig. S13 S-V plot of I_0/I vs. HA concentration in urine.

Table S4. Spiked recoveries and RSDs for the detection of DPP and HA in urine samples.

	Analyte	Added (μM)	Found (μM)	Recovery (%)	RSD (%)
Urine	DPP	0	not detected	–	–
		50	48.30	96.60	5.11
		100	93.66	93.66	3.11
		150	159.65	106.43	3.18
	HA	0	not detected	–	–
		50	46.68	93.36	3.11
		100	95.17	95.17	1.22
		150	156.46	104.31	2.21

Cyclic voltammetry (CV) experiment

Cyclic voltammetry (CV) was carried out on a CHI voltammetric analyzer in a three-electrode cell with a Pt counter electrode, a Ag/AgCl reference electrode, and a glassy carbon working electrode at a scan rate of 100 mVs⁻¹ with 0.1 M tetrabutylammonium hexafluorophosphate, in anhydrous dichloromethane solution purged with nitrogen. The the highest occupied molecular orbital (HOMO) energy level of **1** was estimated on the basis of the onset oxidation potential ($E_{\text{ox}} = -0.896$ eV) in CV of **1** and oxidation potential of -4.8eV with respect to the vacuum level for ferrocene/ferrocenium (Fc/Fc⁺).^{S9} The HOMO was calculated to be about -3.530 eV, according to the following equation: HOMO = -(4.8 + E_{ox} –

$E_{\text{ox(Fc/Fc}^+)$ eV. The lowest unoccupied molecular orbital (LUMO) energy level was estimated to about 0.470 eV, according to the equation $E_{\text{LUMO}} = E_{\text{HOMO}} + E_g$ (E_g estimated from optical absorption band edge).

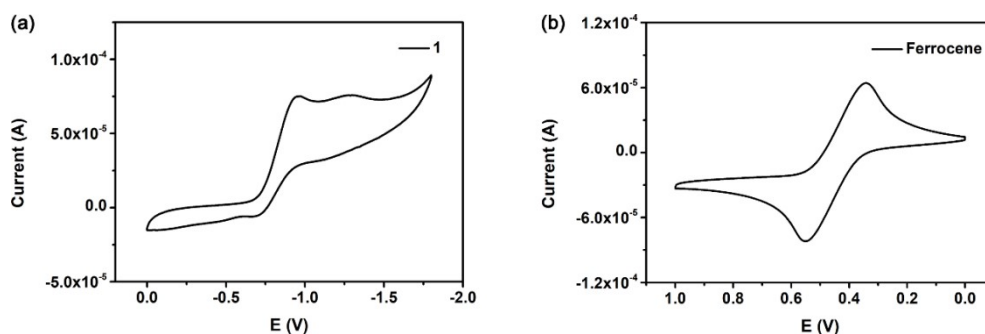


Fig. S14 (a) The CV curve of **1**. (b) The CV curve of ferrocene at room temperature.

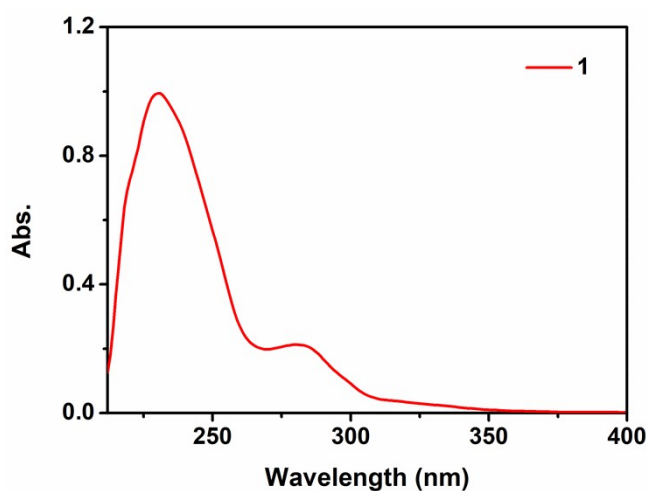


Fig. S15 The UV-Vis spectrum of **1** in dichloromethane.

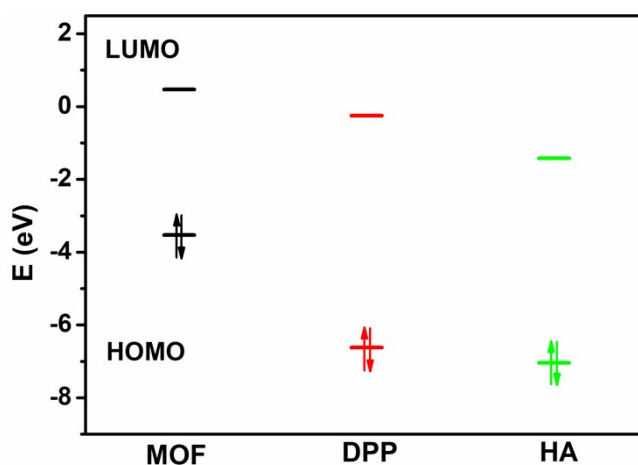


Fig. S16 HOMO and LUMO energies for **1**, DPP, and HA.

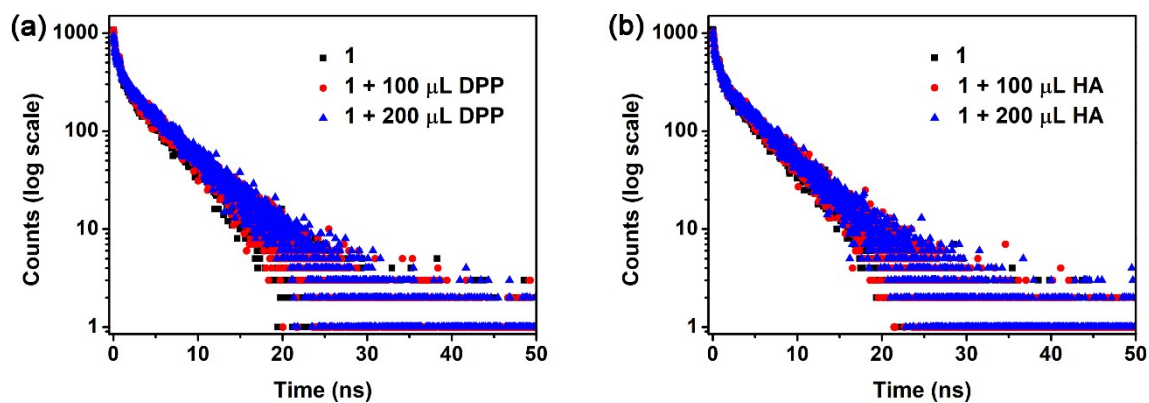


Fig. S17 Time-resolved luminescence decay of **1** before and after addition of (a) DPP and (b) HA.

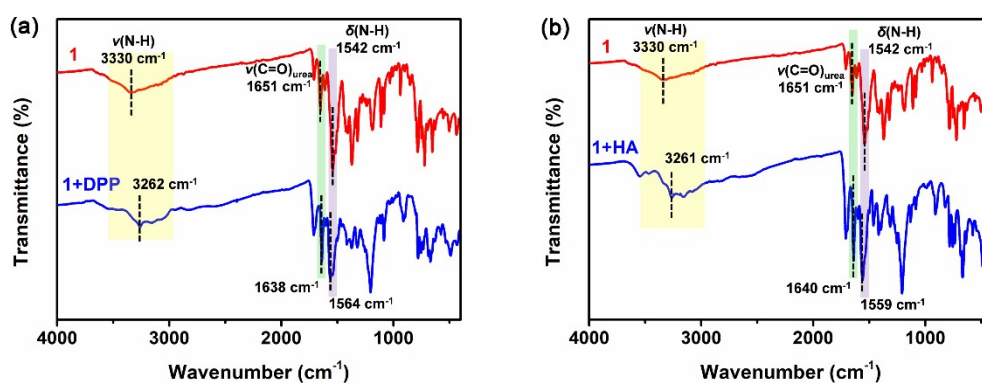


Fig. S18 FT-IR spectra of (a) **1** and **1**+DPP as well as (b) **1** and **1**+HA.

References

- S1 M. C. Naranthatta, S. Bandi, R. Jagan, and D. K. Chand, *Cryst. Growth Des.*, 2016, **16**, 6722–6728.
- S2 G. M. Sheldrick, *Acta Cryst.*, 2015, **C71**, 3–8.
- S3 A. L. Spek, *J. Appl. Crystallogr.*, 2003, **36**, 7–13.
- S4 X. L. Qu and B. Yan, *Inorg. Chem.*, 2020, **59**, 15088–15100.
- S5 J. J. Zhao, L. Zhang, P. Y. Liu, W. Z. Chen, Z. L. Liu and Y. Q. Wang, *Dalton Trans.*, 2021, **50**, 553–561.
- S6 J. N. Hao and B. Yan, *Chem. Commun.*, 2015, **51**, 14509–14512.
- S7 S. J. Qin, J. N. Hao, X. Y. Xu, X. Lian and B. Yan, *Sens. Actuators, B*, 2017, **253**, 852–859.
- S8 Y. R. Du, X. Q. Li, H. J. Zheng, X. J. Lv and Q. Jia, *Anal. Chim. Acta*, 2018, **1001**, 134–142.
- S9 J. Pommerehne, H. Vestweber, W. Guss, R. F. Mahrt, H. Bässler, M. Porsch and J. Daub, *Adv. Mater.*, 1995, **7**, 551–554.